J Eng Math (2015) 95:359–380
DOI 10.1007/s10665-014-9779-1

Bridged defects in continuously and discretely reinforced solids

A. P. S. Selvadurai

Received: 9 July 2014 / Accepted: 22 December 2014 / Published online: 13 March 2015

Abstract The paper examines problems that relate to defects in elastic solids that are reinforced by aligned fibres. The category of problems deals with flaw bridging that can occur as a result of continuity of fibres across the defect in the matrix region. The defects can be a flaw of finite dimensions or cracks in the conventional sense. The presence of fibre continuity across a flaw exerts a displacement-dependent boundary condition at the faces of the crack that can alter the stress state at the boundary of the defect and contribute to fracture generation. The analysis of both a spheroidal flaw with fibre bridging and an idealized penny-shaped crack with fibre continuity across the faces of the crack leads to the conclusion that the stress amplification usually associated with extension of the flaw is suppressed by the fibre continuity. The second type of problem deals with the mechanics of flaws that can emanate from the extremities of an isolated cylindrical fibre in an elastic matrix of infinite extent. The problem is examined using a computational approach based on the boundary integral equation technique. The modelling is used to examine the role of the fibre–matrix elasticity mismatch on the stress intensity factors at the tip of penny-shaped cracks emanating from the ends of the fibre.

Keywords Bridged cracks · Bridged penny-shaped defects · Cracks at fibre ends · Fibre-reinforced composites · Integral equation methods · Stress intensity factors

1 Introduction

In engineering applications, multi-directional reinforcement constitutes the norm, particularly in applications where structures can be subjected to loadings, the directions of which are unspecified. It is less common to use unidirectional reinforcement. However, studying unidirectionally-reinforced materials offers a greater understanding of how the micro-mechanical features can influence load transfer at the fibre-scale. Ideally, fibre-reinforced materials are manufactured to be free of defects, but this is almost impossible to achieve; even ‘perfect’ fibre reinforcement can contain defects introduced during the manufacturing or utilization stages. For example, curing or practical situations such as localized loads, impact loads, extreme temperatures, moisture influx and chemical reactions can affect the integrity of the fibre-reinforced material by compromising the bond at the fibre–matrix interface. Therefore the

A. P. S. Selvadurai (✉)
Department of Civil Engineering and Applied Mechanics, McGill University, 817 Sherbrooke Street West,
Montreal, QC H3A 0C3, Canada
e-mail: patrick.selvadurai@mcgill.ca

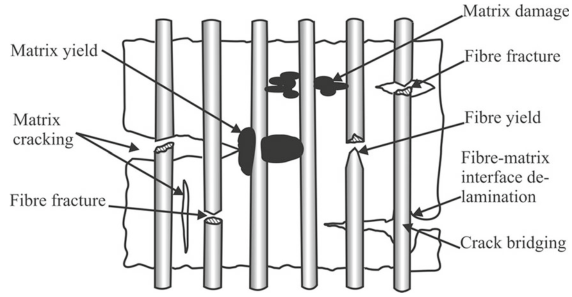

Fig. 1 Defects in a unidirectionally reinforced elastic composite

reliability of the fibre-reinforced material can be influenced by the development of fibre yield, fibre breakage, fibre pullout, matrix fracture, delamination of the fibre–matrix interface, void growth in the matrix, etc. (Fig. 1). Several decades ago, researchers began to discuss the importance of understanding how damage to fibre-reinforced materials can affect their integrity (see, e.g. Backlund [1]). The term flaw bridging was coined to describe situations where intact fibres are able to provide a bridging action capable of facilitating load transfer in situations where the matrix of the material has been damaged or fractured. The effectiveness of such flaw bridging will depend upon the mode of loading of a composite. Since unidirectional reinforcement is intended to enhance the ability to carry loads aligned with the fibre direction, we will examine the processes of flaw bridging for situations where the bridging action is in the same direction as the applied loadings.

The topics of crack and flaw bridging in unidirectional fibre-reinforced composites were discussed by Kelly [2], Aveston and Kelly [3], Bowling and Groves [4], Sih [5], Beaumont and Harris [6] and Beaumont [7]. The initial investigations dealing with the modelling of flaw bridging in composites were presented by Selvadurai [8,9], followed by the work of Stang [10]. Several others, including Rose [11], McCartney [12], Budiansky et al. [13], Budiansky and Amazigo [14], Movchan and Willis [15,16], have investigated various aspects of the elastostatic problem of bridging-induced behaviour of flaws in unidirectional fibre-reinforced materials. Of related interest are the studies in the area of fibre-reinforced cementitious materials where bridging action is an essential part of the mechanisms associated with the generation of the load-carrying capacity. The literature in this field is vast, and no attempt is made to provide a comprehensive literature survey. Accounts of developments in this area are given in [17–24].

As a demonstration of the impact of flaw bridging, the paper first considers the problem of the bridging of an oblate spheroidal cavity related to a unidirectionally reinforced composite, where the fibres are exposed in the spheroidal region and exhibit continuity across the faces of the flaw [25]. The mechanical behaviour of the unidirectionally reinforced composite is treated as a transversely isotropic elastic solid, and the equatorial plane of the spheroidal cavity is assumed to be aligned with the plane of transverse isotropy of the composite. The analysis of the bridged spheroidal cavity problem uses the results for spheroidal defects in transversely isotropic elastic solids developed by Chen [26], which yields a compact analytical result for the stress concentration at the boundary of the spheroidal defect. Other bridging fibre orientations can be considered, but the greatest benefit from the bridging action is derived when the fibres are aligned normal to the equatorial plane of the defect and the loading of the transversely isotropic solid is along the axis of elastic symmetry.

The problem of a penny-shaped crack in an *isotropic elastic solid* where the surfaces of the crack are subjected to displacement-dependent tractions was first considered by Atkinson [27]. The displacement-dependent boundary conditions are a form of “bridging” that can influence the stress intensity factors at the crack tip. The problem of a bridged penny-shaped crack in a transversely isotropic elastic solid [8,9] is relevant to examining the bridging action across penny-shaped flaws in unidirectionally fibre-reinforced solids. The general approach can also be used to examine bridged Griffith cracks and edge cracks in composite plates [28] and locally loaded bridged external cracks in composite solids [29]. The bridging action across defects located in composite materials is amenable to mathematical modelling only in special situations where the external loading of the unidirectionally reinforced composite does not induce a state of compression in the bridging fibre region. In problems where the displacement-dependent tractions of the bridging fibres exhibit a unilateral character, the analysis of the associated mixed boundary value problem related to the crack will also involve the identification of the boundary of the region that imposes the displacement-dependent traction boundary conditions. This class of problems is best analysed through an iterative computational approach.

One category of fibre-reinforced composite material employs the reinforcement of a brittle matrix by randomly distributed fibres of finite length. The objective of short-fibre-reinforcement is to suppress the development of damage and fracture in the brittle matrix [30–32]. The development of interface delamination between a reinforcing fibre and the brittle elastic matrix can be accomplished through the use of bond-enhancing agents. Experimental evidence suggests that matrix cracking can originate both at the extremities of the reinforcing fibre of finite length and at locations where the fibre itself experiences fracture. Problems related to the interaction of matrix cracks and discrete fibre reinforcement have been examined in the literature. Pacella and Erdogan [33] investigated the mechanics of a penny-shaped crack located within a symmetric arrangement of discrete reinforcing fibres. Wijeywickrema et al. [34] examined the problem of the axial loading of a single fibre composite region containing an annular crack, which is an extension to the study of the classical problem of an annular crack in an extended elastic solid [35,36]. The role of the fibre in attenuating the Mode I stress intensity factor at the interior tip of the annular crack is examined. The study of this category of problem requires the micro-mechanical modelling of individual fibres and the defects that originate at fibre extremities. The problem can also be examined by representing the fibre as a prolate spheroidal elastic inclusion in an elastic matrix where cracks can originate in the vicinity of the extremities of the inclusion. A problem of this type was examined by Taya and Mura [37] who examined the uniaxial stressing of an aligned short-fibre reinforced composite containing fibre end cracks. Selvadurai et al. [38] examined the axisymmetric problem of the uniform axial stressing of a single fibre–infinite matrix region, which contains a penny-shaped crack through the matrix. The analysis is reduced to a set of coupled integral equations of the Fredholm-type that can be solved only in a numerical fashion. The analytical results are used to confirm the accuracy of a boundary element analysis of the identical problem. The boundary element technique was successfully applied by ten Busschen and Selvadurai [39] and Selvadurai and ten Busschen [40] to examine the problem of matrix crack extension at the site of a single broken fibre embedded in a brittle matrix. The computational approach is used to predict the mode of matrix crack extension. Other computational techniques have been used to examine fracture mechanics problems where singular fields at the crack tip are modelled correctly. The primary advantage of the boundary element approach is the ability to examine the process of crack extension without re-meshing the domain [40,41]. The technique therefore offers the possibility of matrix crack extension at arbitrary orientations from fractured fibre locations. Considering the advantages of the boundary element scheme, the present paper applies the axisymmetric boundary element technique to examine the problems related to the axial stressing of a single cylindrical elastic short fibre embedded in an elastic matrix with penny-shaped delaminations at the extremities of the fibre. The boundary element technique is used to determine the Mode I and Mode II stress intensity factors at the tip of the penny-shaped crack. The influence of the fibre–matrix modular ratio in amplifying the stress intensity factors at the crack tip is demonstrated. The boundary element technique is also used to examine the problem where a fractured fibre gives rise to a penny-shaped crack. The influence of the axial loading of the fibre in amplifying the Mode I stress intensity factor is investigated.

2 Elastic modelling of unidirectionally reinforced solids

Unidirectionally fibre-reinforced materials in their fabricated condition generally consist of a weaker and usually brittle matrix that is reinforced by stronger fibres that are separated and regularly arranged to provide a composite with a continuous fibre–matrix bond. This is admittedly an oversimplified idealization; the fibre arrangement is often irregular [42] (Fig. 2) resulting in contact between the fibres, which could initiate defects in the material. Mathematical and mechanics-based theories have been developed to model composites with unidirectional fibre reinforcement; these treatments have led to the consideration of more complicated arrangements of fibre reinforcement. The research articles by Spencer [43–46] give examples of the use of the classical theory of ideal

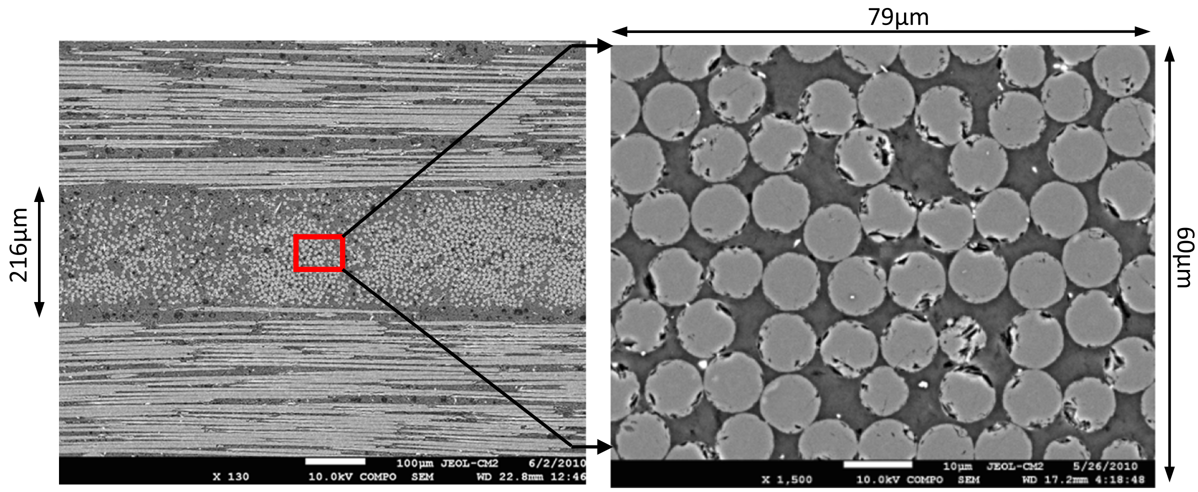

Fig. 2 Scanning Electron Microscope view of a multi-laminate fibre-reinforced plate and the detail of the fibre configuration [42]

fibre-reinforced solids, while Hill [47], Hashin and Rosen [48], Hale [49] and Christensen [50] give accounts of the developments in the theory of composites.

We consider a unidirectionally reinforced elastic solid, which can be modelled as a transversely isotropic elastic solid with the plane of transverse isotropy normal to the fibre direction, following Elliott [51], Shield [52], Chen [26], Lekhnitskii [53] and Green and Zerna [54]. Referring to the axisymmetric cylindrical polar coordinate system (r, z), it can be shown that the displacement and stress fields in the transversely isotropic elastic medium can be expressed in terms of two functions: $\varphi_\alpha(r, z)$ $(\alpha = 1, 2)$, which are solutions of

$$\left(\frac{\partial^2}{\partial r^2} + \frac{1}{r}\frac{\partial}{\partial r} + \frac{\partial^2}{\partial z_\alpha^2}\right)\varphi_\alpha(r, z) = 0, \tag{1}$$

where $z_\alpha = z/\sqrt{n_\alpha}$ and n_α are the roots of the characteristic equation

$$c_{11}c_{44}n^2 + \{c_{13}(2c_{44} + c_{13}) - c_{11}c_{33}\}n + c_{33}c_{44} = 0. \tag{2}$$

In (2), c_{ij} are the elastic constants of the transversely isotropic elastic model of the unidirectionally fibre-reinforced solid. These elastic constants can be expressed in terms of the isotropic elastic constants of the fibre (suffix f) and the matrix (suffix m) phases and their respective volume fractions (i.e. E_f, ν_f, E_m, ν_m and V_f and V_m, respectively). These expressions are given by Hashin and Rosen [48], and a summary of the expressions is given in the Appendix. The eigenvalues of (2) may be real or complex depending on the elastic constants c_{ij} (see, e.g. [26,51–54]). The displacement and stress fields in the transversely isotropic elastic material can be expressed in terms of $\varphi_\alpha(r, z)$ as follows:

$$\{u_r(r, z); u_z(r, z)\} = \sum_{\alpha=1}^{2}\left\{\frac{\partial\varphi_\alpha}{\partial r};\ \frac{k_\alpha}{\sqrt{n_\alpha}}\frac{\partial\varphi_\alpha}{\partial z_\alpha}\right\} \tag{3}$$

and

$$\sigma_{rr} = c_{44}\sum_{\alpha=1}^{2}\left(\frac{1+k_\alpha}{n_\alpha}\left\{\frac{\partial^2}{\partial r^2} + \frac{1}{r}\frac{\partial}{\partial r}\right\}\varphi_\alpha - \frac{c_{11}-c_{12}}{c_{44}}\frac{1}{r}\frac{\partial\varphi_\alpha}{\partial r}\right), \tag{4}$$

Fig. 3 Spheroidal flaw with fibre bridging in the unidirectionally fibre-reinforced composite material

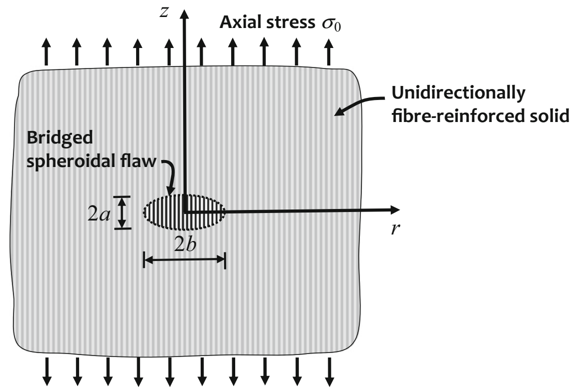

$$\sigma_{\theta\theta} = c_{44}\sum_{\alpha=1}^{2}\left(\frac{1+k_\alpha}{n_\alpha}\left\{\frac{\partial^2}{\partial r^2}+\frac{1}{r}\frac{\partial}{\partial r}\right\}\varphi_\alpha - \frac{c_{11}-c_{12}}{c_{44}}\frac{\partial^2\varphi_\alpha}{\partial r^2}\right), \tag{5}$$

$$\sigma_{zz} = c_{44}\sum_{\alpha=1}^{2}\frac{\partial^2\varphi_\alpha}{\partial z_\alpha^2}, \tag{6}$$

$$\sigma_{rz} = c_{44}\sum_{\alpha=1}^{2}\left\{\frac{1+k_\alpha}{\sqrt{n_\alpha}}\frac{\partial^2\varphi_\alpha}{\partial r\,\partial z_\alpha}\right\}, \tag{7}$$

where

$$k_\alpha = \frac{c_{11}n_\alpha - c_{44}}{c_{13}+c_{44}},\ \ (\alpha = 1, 2). \tag{8}$$

3 The bridged spheroidal defect

As a prelude to the discussion of the flaw bridging action in a unidirectionally fibre-reinforced solid, we consider the three-dimensional problem in which an oblate spheroidal region contains only fibres. The equatorial plane of the oblate spheroidal cavity is assumed to coincide with the plane of transverse isotropy of the unidirectionally fibre-reinforced solid. The exposed fibres exert a displacement-dependent traction boundary condition at the boundary of the cavity. The unidirectionally reinforced solid containing the aligned bridged spheroidal flaw is subjected to a uniaxial state of stress, which is oriented in the fibre direction (Fig. 3). The boundary of the spheroidal flaw is described by the equation:

$$\frac{z^2}{a^2}+\frac{r^2}{b^2} = 1, \tag{9}$$

where a and b are, respectively, the semi-minor and semi-major axes of the spheroidal region and the axis z is aligned with the fibre direction. We consider a fibre composite region B bounded internally by the fibre region. At the boundary of the fibre region ∂B, (i) there is continuity of displacement between the fibre domain (superscript f) and the composite region (superscript c); (ii) there is the continuity of traction in the z-direction; (iii) since the fibres can exert a traction only in their alignment direction, there is zero radial traction on the surface of the spheroidal cavity; and (iv) at locations remote from the spheroidal cavity, the stress field should reduce to a uniaxial stress state. These are equivalent to the following conditions:

$$u_z^f(r,z) = u_z^c(r,z) \quad \text{for} \quad (r,z)\in\partial B, \tag{10}$$

$$T_z^f(r,z) = T_z^c(r,z) \quad \text{for} \quad (r,z) \in \partial B, \tag{11}$$

$$T_r^c(r,z) = 0 \quad \text{for} \quad (r,z) \in \partial B, \tag{12}$$

$$\sigma_{zz}^c(r,z) = T_0 \quad \text{for} \quad (r,z) \in B. \tag{13}$$

For the solution of the bridged spheroidal flaw problem, it is convenient to adopt a solution technique where a combination of solutions are used, with one solution corresponding to the uniaxial stress state and the second solution accounting for the effects of the bridged spheroidal flaw. The combined solution for the displacement field is given by

$$u_r^c(r,z) = -\frac{T_0 c_{13} r}{\chi} + u_r^*(r,z), \tag{14}$$

$$u_z^c(r,z) = -\frac{T_0(c_{11}+c_{12})z}{\chi} + u_r^*(r,z) \tag{15}$$

and

$$\sigma_{rr}^c(r,z) = \sigma_{rr}^*(r,z), \tag{16}$$

$$\sigma_{\theta\theta}^c(r,z) = \sigma_{\theta\theta}^*(r,z), \tag{17}$$

$$\sigma_{zz}^c(r,z) = T_0 + \sigma_{zz}^*(r,z), \tag{18}$$

$$\sigma_{rz}^c(r,z) = \sigma_{rz}^*(r,z), \tag{19}$$

where

$$\chi = c_{33}(c_{11}+c_{12}) - 2c_{13}^2. \tag{20}$$

The displacement and stress fields associated with u_i^* and σ_{ij}^* can be determined by introducing a new variable $q(r,z)$ defined by the equation

$$\frac{z^2}{q^2} + \frac{r^2}{q^2-1} = c^2 \qquad \text{where} \qquad c^2 = a^2 - b^2. \tag{21}$$

The surfaces, $q = \text{const.}$, represent a spheroid in the (r,z) space, and the functions $q_\alpha(r, z_\alpha)$, $(\alpha = 1, 2)$ are defined by the relationships:

$$\frac{z_\alpha^2}{q_\alpha^2} + \frac{r^2}{q_\alpha^2-1} = c_\alpha^2, \ (\alpha = 1,2) \tag{22}$$

with

$$c_\alpha^2 = a_\alpha^2 - b^2, \quad a_\alpha^2 = \frac{a^2}{n_\alpha}, \tag{23}$$

and the applicability of the preceding representations for modelling spheroidal regions in transversely isotropic media is given by Chen [26]. The result (22) is useful in subsequent developments. Also, when

$$q_\alpha = \rho_\alpha, \quad \rho_\alpha = \frac{\Gamma^2}{\Gamma^2 - n_\alpha}, \quad \Gamma = \frac{a}{b}, \tag{24}$$

the appropriate displacement and stress field corresponding to $u_i^*(r,z)$ and $\sigma_{ij}^*(r,z)$ in the composite region can be obtained by selecting a potential function of the form [26]:

$$\varphi_\alpha(r,z) = \frac{A_\alpha}{2}\left[z_\alpha^2\left(\tfrac{1}{2}\ln\left(\tfrac{q_\alpha+1}{q_\alpha-1}\right) - \tfrac{1}{q_\alpha}\right) + r^2\left(-\tfrac{1}{4}\ln\left(\tfrac{q_\alpha+1}{q_\alpha-1}\right) + \tfrac{q_\alpha}{2(q_\alpha^2-1)}\right) - \tfrac{c_\alpha^2}{2}\ln\left(\tfrac{q_\alpha+1}{q_\alpha-1}\right)\right], \tag{25}$$

where A_α are arbitrary constants.

For the fibrous flaw region F, (which is contained within the unidirectionally reinforced composite region B), the variation in the axial displacement $u_z^f(r,z)$ takes the general form:

$$u_z^f(r,z) = zS(r), \quad (r,z) \in F, \tag{26}$$

where $S(r)$ is an arbitrary function. Since the fibrous flaw region is incapable of sustaining radial and shear stresses,

$$\sigma_{rr}^f(r,z) = \sigma_{rz}^f(r,z) = 0, \quad (r,z) \in F \tag{27}$$

and

$$T_z^f(r,z) = E_f V_f S(r) n_z, \quad (r,z) \in \partial B. \tag{28}$$

Note that the parameter V_f appearing in (28) accounts for the fact that effective fibre elasticity in the fibrous spheroidal inclusion region is volume averaged. The absence of the factor V_f would imply that the entire fibrous inclusion region is composed of material with elasticity E_f. In (28), n_z is the direction cosine of the normal to the spheroidal interface ∂B or $q = \rho$, with

$$n_r = \frac{r}{(\rho^2-1)D_0}, \quad n_z = \frac{z}{\rho^2 D_0}, \quad D_0^2 = \frac{r^2}{(\rho^2-1)^2} + \frac{z^2}{\rho^4}. \tag{29}$$

The solution procedure for the spheroidal fibrous flaw problem is straightforward [25] and involves the application of the continuity of the axial displacement, continuity of axial traction and null radial traction boundary condition on the fibrous inclusion boundary ∂B to eliminate the unknown function $S(r)$ and to determine the unknown constants A_α $(\alpha = 1, 2)$. The influence of the bridging action is best illustrated by examining the amplification of the circumferential stress at the boundary of the equatorial plane. Omitting details, it can be shown that for real values, the expression for the axial stress takes the form:

$$\frac{\sigma_{zz}(r,0)}{T_0} = 1 + \sum_{\alpha=1}^{2} \lambda_\alpha (1+k_\alpha)\left(\frac{1}{2}\ln\left(\frac{q_\alpha^0+1}{q_\alpha^0-1}\right) - \frac{1}{q_\alpha^0}\right), \tag{30}$$

where the superscript 'c' has been omitted for convenience and

$$\begin{aligned}
&\lambda_1 = \zeta\lambda_2, \quad \zeta = -\frac{\frac{1+k_2}{n_2}\Psi_1(\rho_2) + \frac{c_{11}-c_{12}}{c_{44}}\Psi_2(\rho_2)}{\frac{1+k_1}{n_1}\Psi_1(\rho_1) + \frac{c_{11}-c_{12}}{c_{44}}\Psi_2(\rho_1)},\\
&\lambda_2 = \frac{1-\xi\Omega}{\Omega\left\{\frac{k_1}{n_1}\zeta\Psi_1(\rho_1) + \right\}\frac{k_2}{n_2}\zeta\Psi_1(\rho_2) + 2(1+k_1)\zeta\Psi_2(\rho_1) + 2(1+k_2)\zeta\Psi_2(\rho_2)},\\
&\xi = \frac{c_{44}(c_{11}+c_{12})}{c_{33}(c_{11}+c_{12}) - 2c_{13}^2},\\
&\Psi_1(\rho_i) = \frac{1}{2}\ln\left(\frac{\rho_i+1}{\rho_i-1}\right) - \frac{1}{\rho_i}, \quad \Psi_2(\rho_i) = -\frac{1}{4}\ln\left(\frac{\rho_i+1}{\rho_i-1}\right) + \frac{\rho_i}{2(\rho_i^2-1)}.
\end{aligned} \tag{31}$$

Expression (30) can be evaluated for a specific choice of a fibre-reinforced composite where the effective transversely isotropic properties are determined from the effective elasticity estimates for unidirectionally reinforced composites developed by Hashin and Rosen [48], which are summarized in the Appendix. In general, the parameters k_α, n_α, λ_α

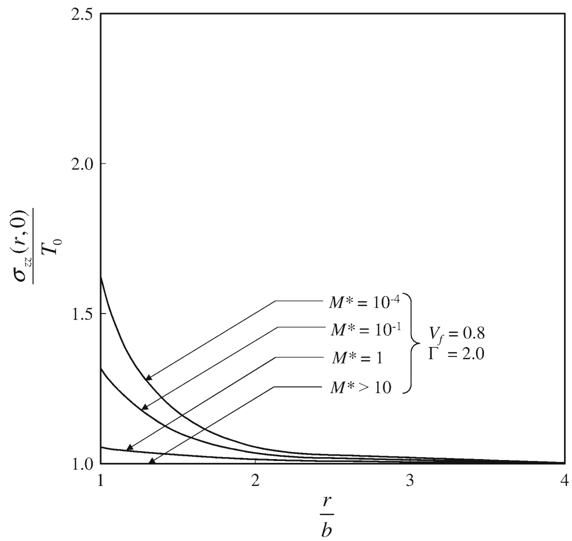

Fig. 4 Axial stress distribution in the unidirectional fibre-reinforced composite on the equatorial plane of the prolate spheroidal flaw with fibre bridging ($\Gamma = 2.00$)

and the functions $\Psi_\beta(q_\alpha)$ ($\beta = 1, 2$) can be real- or complex-valued depending on the elastic constants c_{ij}. As a result, the distribution of axial stress on the equatorial plane needs to be evaluated by considering the result:

$$\frac{\sigma_{zz}(r,0)}{T_0} = 1 + \mathrm{Re}\left\{\sum_{\alpha=1}^{2} \lambda_\alpha (1 + k_\alpha)\left(\frac{1}{2}\ln\left(\frac{q_\alpha^0 + 1}{q_\alpha^0 - 1}\right) - \frac{1}{q_\alpha^0}\right)\right\}. \tag{32}$$

To present certain numerical results, we consider the specific case of a unidirectionally fibre-reinforced material where the matrix properties are as follows: $E_m = 27.6$ GPa, $\nu_m = 0.35$ and $\nu_f = 0.20$. The elastic modulus of the fibre is varied as a multiple of the elasticity of the matrix, i.e. $E_f = M^* E_m$. Also the specification of the volume fraction of the fibres V_f completes the description of the fibre-reinforced composite. The geometry of the fibrous flaw is specified by the flaw aspect ratio $\Gamma = a/b$ which is assigned values corresponding to a prolate ($\Gamma = 2.0$) and oblate ($\Gamma = 0.5$) spheroidal region, respectively. Figs. 4 and 5 illustrate typical variations in the axial stress distribution within the composite region for spheroidal cavities as a function of the fibre–matrix modular ratio M^*. As the spheroidal fibrous-bridging region acquires an oblate shape, the stress concentration at the boundary of the cavity is amplified. In the limit as the oblate spheroidal region flattens to a crack, the stress at the boundary of the crack will become singular, and the singularity will be suppressed as the elasticity of the reinforcing fibres increases. The influence of the bridging action on the development of stress amplification at the boundary of the spheroidal region is illustrated in Fig. 6. As is evident, the elastic stiffness of the bridging fibres has a significant influence in moderating the stress amplification and when $M^* > 10^2$, which is satisfied by most reinforcing materials, the stress amplification is significantly reduced.

4 The bridged penny-shaped crack problem

The analytical solution for the axisymmetric problem of a penny-shaped crack located in an isotropic elastic solid of infinite extent was presented by Sack [55] and Sneddon [56] using spheroidal function and dual integral equation formulations, respectively. The analytical solution can be used to develop an exact result for the Mode I stress intensity factor at the crack tip, and the result has been extensively used in fracture mechanics calculations (see e.g. Liebowitz [57], Sih [58], Cherepanov [59]) and for benchmarking computational treatments of fracture mechanics problems. In this section, we examine the problem of the bridged penny-shaped crack problem for a transversely isotropic elastic solid, which introduces a displacement-dependent normal traction constraint on the faces of the

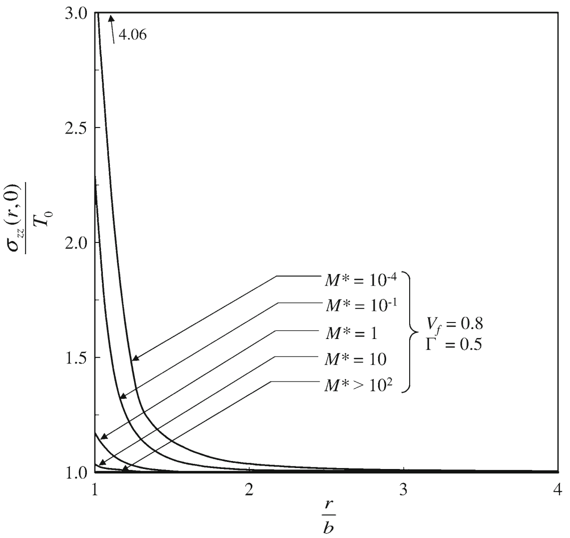

Fig. 5 Axial stress distribution in the unidirectional fibre-reinforced composite on the equatorial plane of the oblate spheroidal flaw with fibre bridging ($\Gamma = 0.50$)

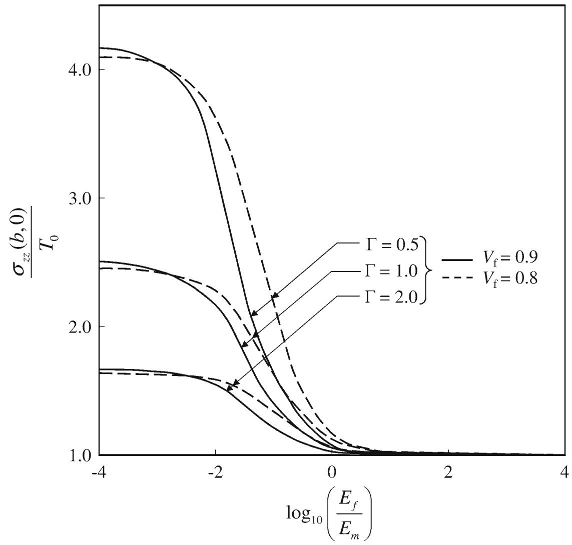

Fig. 6 Stress amplification at the boundary of the bridged spheroidal flaw

crack (Fig. 7). The analysis of penny-shaped cracks with displacement-dependent traction boundary conditions on the crack faces was first examined by Atkinson [27] using an iterative technique. We examine the problem of a penny-shaped matrix crack that is located in a unidirectional fibre-reinforced material, where the fibres exhibit continuity across the faces of the crack. To preserve axial symmetry in the problem, the plane of the penny-shaped matrix crack is selected normal to the direction of uniaxial reinforcement, and we introduce the assumption that the bridging fibres have a constant length within the penny-shaped debonded region. This assumption gives rise to a displacement constraint which is derived from a fibre that has a finite length at the crack tip. This assumption can be modified by assuming a variation of the debonded length that varies from a finite value at the centre of the penny-shaped crack to zero at the boundary. This introduces a further variable in terms of the nature of the distribution of the lengths of constraining ligaments within the penny-shaped crack region. Comments related to the improvement of the description of the distribution of fibre length within the crack region will be discussed later in this section. The axisymmetric bridged crack problem can be formulated in relation to a halfspace region, where the surface of the halfspace region is subjected to mixed boundary conditions:

$$u_z(r,0) = 0\,, \quad b \le r < \infty, \tag{33}$$

$$\sigma_{zz}(r,0) = -p^*(r) + \frac{E_f V_f}{l} u_z(r,0); \quad 0 < r < b, \tag{34}$$

$$\sigma_{rz}(r,0) = 0; \quad 0 \le r \le \infty, \tag{35}$$

where $p^*(r)$ is the tensile traction induced in the plane $z = 0$ of the intact composite due to the action of the external stress state. Again, we note that elasticity of the bridging fibre is modified by the factor V_f to ensure that the region is not completely occupied by the elastic fibres. For the analysis of the mixed boundary value problem posed by (33)–(35), we seek solutions of (1), which are based on Hankel transform developments (Sneddon [60], Selvadurai [61]). The relevant solutions that satisfy the regularity conditions applicable to a halfspace region are

$$\varphi_i(r,z) = \frac{1}{b^2}\int_0^\infty \xi A_i(\xi) \mathrm{e}^{-\eta_i z} J_0(\xi r/b)\mathrm{d}\xi, \tag{36}$$

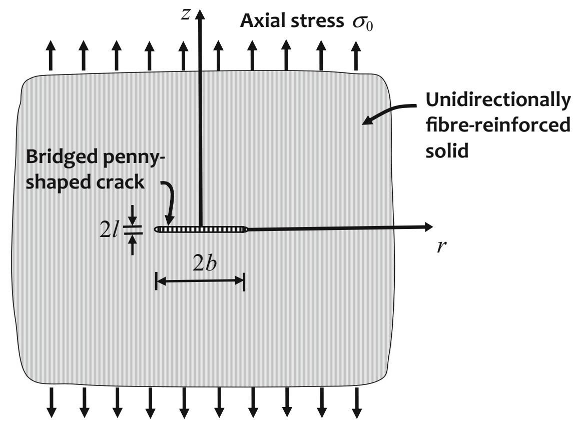

Fig. 7 Bridged penny-shaped crack

where $A_i(\xi)$ are arbitrary functions and $\eta_i = \xi/b\sqrt{\nu_i}$. The mixed boundary conditions (33) to (35) can be reduced to a system of dual integral equations for a single unknown function. Using a finite Fourier transform, we can further reduce the dual system to a single Fredholm integral equation of the second-kind for an unknown function $\phi(t)$, which takes the form

$$\phi(t) - \frac{\beta}{\pi}\int_0^1 K(t,\tau)\phi(\tau)\,\mathrm{d}\tau = g(t), \tag{37}$$

where

$$K(t,\tau) = 2\int_0^\infty \vartheta^{-1}\sin(\vartheta t)\sin(\vartheta\tau)\mathrm{d}\vartheta$$
$$\beta = \frac{E_f V_f b\sqrt{\nu_1\nu_2}(k_1-k_2)}{E_m l\Omega^*}; \quad \Omega^* = \frac{\Omega c_{44}}{E_m}, \tag{38}$$
$$\Omega = \sqrt{\nu_1}(1+k_1)\left(\frac{k_2c_{33}-\nu_2c_{13}}{c_{44}}\right) - \sqrt{\nu_2}(1+k_2)\left(\frac{k_1c_{33}-\nu_1c_{13}}{c_{44}}\right).$$

The function $g(t)$ depends only on the nature of the axisymmetric external loading. For example, when the composite is subjected to a uniform tensile stress field at infinity

$$g(t) = t. \tag{39}$$

It should be noted the function $\phi(t)$ will contain a multiplier that takes into account the magnitude and nature of the loading. The mathematical analysis of the bridged penny-shaped crack problem (for $t \in$ real and $\tau \in$ real) is formally reduced to the solution of

$$\phi(t) - \frac{\beta}{\pi}\int_0^1 \ln\left(\frac{t+\tau}{t-\tau}\right)\phi(\tau)\,\mathrm{d}\tau = g(t); \quad t > \tau \geq 0. \tag{40}$$

The integral equation (40) can be classified as a Fredholm type, even though the kernel suffers a discontinuity at $t = \tau$, since the kernel is quadratic integrable (Mikhlin [62]):

$$\int_0^1\int_0^1 \ln|t-\tau|\,\mathrm{d}t\mathrm{d}\tau \to \text{finite}.$$

The solution of (40) provides, formally, results of importance to the idealized bridged penny-shaped crack with a bridged region of constant length $2l$ over the entire crack surface. The result of particular interest to fracture mechanics of composites relates to the Mode I stress intensity factor at the crack tip, defined by

$$\mathrm{K_I} = \lim_{r \to b^+} [2(r-b)]^{1/2} \sigma_{zz}(r, 0). \tag{41}$$

Considering the result for the axial stress expressed in terms of $\phi(t)$, it can be shown that for a penny-shaped crack in a unidirectional fibre-reinforced material with crack bridging and subjected to a uniform far-field axial stress σ_0,

$$\mathrm{K_I} = \frac{2\sigma_0\sqrt{b}}{\pi}\phi(1). \tag{42}$$

In the limiting case when the elasticity of the bridging fibres $E_f \to 0$, $\beta \to 0$, and we have a penny-shaped crack located in a matrix with unidirectional cavities where originally there were fibres. Since the resulting material is still transversely isotropic and $\phi(1) = 1$, expression (42) for the stress intensity factor gives

$$\mathrm{K_I} = \frac{2\sigma_0\sqrt{b}}{\pi}, \tag{43}$$

which is the classical result. As the fibre elasticity reduces to zero, the isotropic matrix still retains a transversely isotropic character due to the aligned voids that correspond to the fibres. The stress intensity factor is independent of the transverse isotropy of the medium with directional voids. Consider the limiting case when the unidirectional fibre-reinforced material is reinforced with inextensible fibres (i.e. $E_f \to \infty$): This is an idealization that was proposed by Adkins and Rivlin [63] and successfully developed by Spencer [43], Everstine and Pipkin [64], England and Rogers [65], Pipkin and Rogers [66], Spencer [67], Sanchez and Pipkin [68], Morland [69] and Pipkin [70] for the stress analysis and for examining a wide class of problems in idealized fibre-reinforced materials. In recent years, the theory has been extended by Spencer and Soldatos [71] and Soldatos [72,73] to include fibres that possess bending stiffness.

In the limit, the integral equation (12) reduces to

$$\int_0^1 \ln\left(\frac{t+\tau}{t-\tau}\right)\phi(\tau)\,\mathrm{d}\tau = 0, \tag{44}$$

which has a trivial solution $\phi(t) = 0$. Consequently, $\mathrm{K_I} \equiv 0$, and the stress intensity factor is completely suppressed. The limit, of course, has to be approached with caution since there are boundary layers that can exist in the medium at the crack tip, which can lead to stress channelling phenomena. (i.e. the stresses are transmitted along single inextensible fibres that can carry the stresses [64–70]) For arbitrary values of the elastic properties of the fibre-reinforced composite, the integral equation (40) has a non-degenerate solution. There appears to be no closed form solution of this equation, and the Fredholm integral equation can be solved using quadrature techniques that reduce the integral equation to a matrix equation. Details of the method are well documented in the literature (Baker [74], Delves and Mohamed [75], Atkinson [76], Selvadurai [77–80]). Figure 8 illustrates the influence of the fibre–matrix elastic modular ratio and the geometry of the bridging zone on the Mode I stress intensity factor for the bridged penny-shaped crack. It is evident that as the fibre–matrix modular ratio increases and the bridging region geometry in terms of the fibre length decreases, the Mode I stress intensity factor for the bridged penny-shaped crack decreases. The general modelling approach for examining bridging action at penny-shaped flaws subjected to loading by a dipole of forces is presented in [9], and a similar problem for the bridged external circular crack is given in [29]. Analogous results for the case of the bridged plane crack are also presented in [28]. The assumption of a constant length of a ligament zone is a limitation of the above modelling approach. The modelling can be improved by examining the limiting results observed in the preceding studies and by prescribing the axial displacement in the fibrous region to be of the form:

$$u_z(r,0) = \begin{cases} C_1(b^2-r^2)^2 + C_2(b^2-r^2)^{1/2} & 0 < r \le b, \\ 0 & b < r < \infty, \end{cases} \tag{45}$$

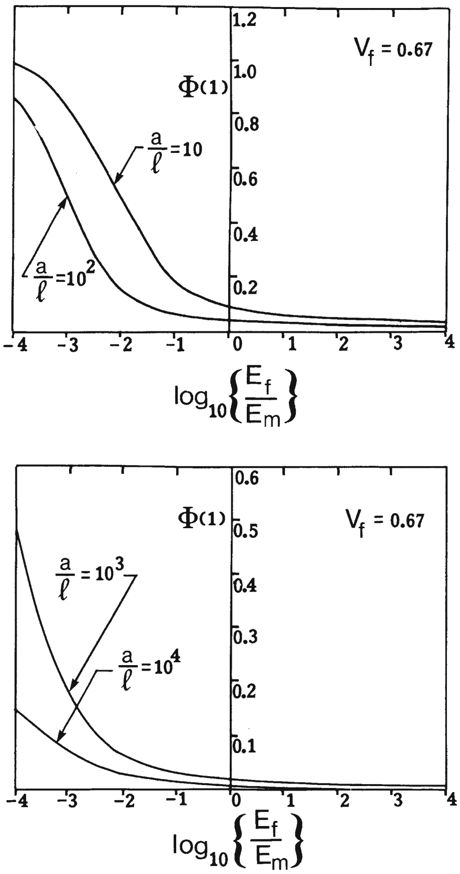

Fig. 8 Mode I stress intensity factor at a bridged penny-shaped crack

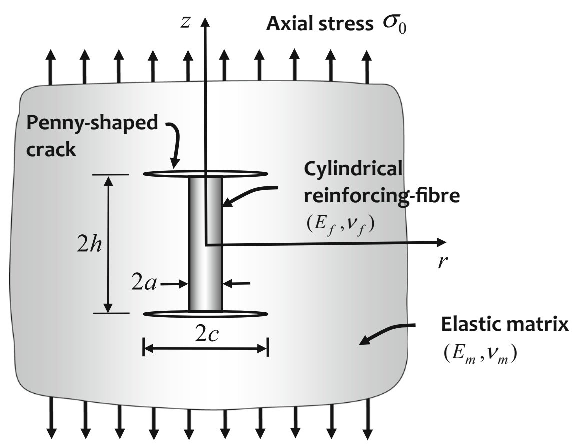

Fig. 9 Cylindrical reinforcing fibre with penny-shaped end cracks

where C_1 and C_2 are arbitrary constants. The axial displacement distribution (45) can accommodate the limiting cases of (i) a crack bridged by relatively stiff fibres, which can result in a zero gradient of the axial displacement distribution at the boundary $r = b$ and (ii) a displacement distribution that will approach the profile of an unconstrained penny-shaped crack at the boundary of the crack, which can correspond to a constraint offered by relatively flexible fibres. The presence of the arbitrary constants allows the application of a variational technique for their determination. The stress distribution corresponding to the prescribed displacement (45) can be obtained by solving a set of mixed boundary value problems for a halfspace region. This enables the development of a total energy potential (U) for the infinite space region, consisting of (i) the elastic energy of the fibre-reinforced region, (ii) elastic energy of the bridging ligaments and (iii) the potential of the external loads, which will be indeterminate within the arbitrary constants C_1 and C_2. These arbitrary constants can be uniquely determined by using the constraints, which represents the minimization of the total potential energy of the system with respect to the arbitrary constants:

$$\frac{\partial U}{\partial C_1} = \frac{\partial U}{\partial C_2}. \tag{46}$$

It has been demonstrated [81–85] that the variational procedure outlined above can be used to examine contact and crack problems where displacements are prescribed in an arbitrary manner and the solutions provide approximate analytical results to problems that can otherwise be examined only by using computational approaches.

5 Cracks at the extremities of fibre inclusions

Reinforcement of both ductile and brittle elastic matrices by random distributions of short-fibre inclusions is used quite extensively to enhance the fracture toughness and fatigue properties of reinforced composites (Spencer [86], Sih and Tamuzs [87], Hashin and Herakovich [88], Kelly and Rabotnov [89], Clyne and Withers [31], Selvadurai [32].) The development of defects in such short fibre composites is therefore an integral part of the stress analysis of such composites. In the case where the fibre has a finite length, defects will usually initiate at the ends of the reinforcing fibres with sharp edges, and this can result in fibres or inclusions with end cracks (Taya and Mura [37], Mura [90], Nemat-Nasser and Hori [91]). The analysis of a representative element of such a short-fibre–brittle elastic matrix containing edge cracks can be complicated by the presence of a bimaterial region, the finite domain of the fibre, the orientation of the defects in relation to the orientation of the short fibre and the type of loading. The problem of the axisymmetric loading of an infinite domain containing a penny-shaped crack across a single fibre was presented in [38], and the resulting mathematical formulation of the elasticity problem required the solution of three coupled integral equations of the Fredholm type, which could only be solved in numerical fashion. The use of computational approaches at the outset therefore presents an attractive approach for examining the problem of a short fibre embedded in an elastic matrix and with penny-shaped end cracks that extend into the elastic matrix. We consider the axisymmetric problem of a cylindrical fibre embedded in bonded contact along the cylindrical surface of the fibre and with identical penny-shaped cracks at the plane ends of the fibre that extend to the elastic matrix (Fig. 9). The computational approaches that can be used to examine this problem are many and varied, ranging from the finite element methods to the extended finite element methods to the boundary integral equation or the boundary element techniques. Here we apply the boundary element technique to solve the problem shown in Fig. 9. The advantage of the boundary element approach in examining this type of problem is the fact that attention is focused on the evaluation of the stress intensity factors at the boundary of the penny-shaped edge cracks.

5.1 Boundary element methods

The formulation of the boundary element method for elastostatic problems is given in [92–97], and in this section we present a brief outline of the relevant equations applicable to a bi-material elastic region. The generalization to a bi-material elastic region will enable the solution of the crack–fibre interaction problem shown in Fig. 9. We consider isotropic elastic materials for which

$$\sigma_{ij}^{(\alpha)} = \lambda_\alpha \delta_{ij} u_{k,k}^{(\alpha)} + \mu_\alpha \left\{ u_{i,j}^{(\alpha)} + u_{j,i}^{(\alpha)} \right\} \tag{47}$$

and the Navier equations are

$$\mu_\alpha \nabla^2 u_i^{(\alpha)} + (\lambda_\alpha + \mu_\alpha) u_{k,ki}^{(\alpha)} = 0, \tag{48}$$

where λ_α and μ_α are Lamé's constants; the subscript or superscript α refers, respectively, to the matrix (m) or fibre (f) regions; u_i and σ_{ij} are, respectively, the displacement components and the stress tensor referred to the rectangular Cartesian coordinate system, x, y, z; $i, j = x, y, z$; $\lambda_\alpha = 2\mu_\alpha \nu_\alpha/(1-2\nu_\alpha)$; ν_α are Poisson's ratios; ∇^2 is Laplace's operator in terms of rectangular Cartesian coordinate system; and δ_{ij} is Kronecker's delta function. The boundary integral equation for the axisymmetric problem pertaining to the fibre–matrix composite region can be written in the form [92–97]

$$c_{lk} u_k^{(\alpha)}(P) + \int_{\Gamma_\alpha} \left\{ P_{lk}^{*(\alpha)}(Q,P) u_k^{(\alpha)}(Q) - u_{lk}^{*(\alpha)}(Q,P) P_k^{(\alpha)}(Q) \right\} \frac{r}{r_i} \mathrm{d}\Gamma = 0, \tag{49}$$

where P corresponds to the field point and Q corresponds to a source point; l and k can be assigned the coordinates r and z referred to the axisymmetric cylindrical polar coordinate system (r, z) where Γ_α is the boundary of the region α; $u_k^{(\alpha)}(Q, P)$ and $P_k^{(\alpha)}(Q, P)$ are, respectively, the displacement and tractions on the boundary Γ_α and $u_{ik}^{*(\alpha)}$; and $P_{ik}^{*(\alpha)}$ are fundamental solutions. Also in (49), c_{lk} are constants defined by

$$c_{lk} = \delta_{lk} + \varphi_{lk}(P), \tag{50}$$

which is zero when the point is outside the body, and δ_{lk} when the point is within the body. In the case of a smooth boundary where the tangent plane is continuous, $\varphi_{lk}(P) = -\delta_{lk}/2$. In other instances, such as corners, the evaluation of $\varphi_{lk}(P)$ can involve complex algebraic operations, and the value can depend on the corner angle and its orientation in space. Procedures for the evaluation of $\varphi_{lk}(P)$are given in [92] and [98]. For the solution of the fibre–matrix interaction, this calculation is not required.

For axial symmetry, the fundamental solutions for the displacement field are given by

$$u_{rr}^{*(\alpha)} = c\left\{\frac{4(1-\nu_\alpha)(\rho^2+\bar{z}^2)-\rho^2}{2r\bar{R}}\right\}K(\bar{m}) - \left\{\frac{(7-8\nu_\alpha)\bar{R}}{4r} - \frac{e^4-\bar{z}^4}{4r\bar{R}^3 m_1}\right\}E(\bar{m}), \tag{51}$$

$$u_{rz}^{*(\alpha)} = c\bar{z}\left\{\frac{(e^2+\bar{z}^2)E(\bar{m})}{2\bar{R}^3 m_1} - \frac{K(\bar{m})}{2\bar{R}}\right\}, \tag{52}$$

$$u_{zr}^{*(\alpha)} = cr_i\bar{z}\left\{\frac{(e^2-\bar{z}^2)E(\bar{m})}{2r\bar{R}^3 m_1} + \frac{K(\bar{m})}{2r\bar{R}}\right\}, \tag{53}$$

$$u_{zz}^{*(\alpha)} = cr_i\left\{\frac{(3-4\nu_\alpha)K(\bar{m})}{\bar{R}} + \frac{\bar{z}^2 E(\bar{m})}{\bar{R}^3 m_1}\right\}, \tag{54}$$

where

$$\begin{aligned} &\bar{z} = z - z_i; \quad \bar{r} = r + r_i; \quad \rho^2 = r^2 + r_i^2 \\ &e^2 = r^2 - r_i^2; \quad \bar{R}^2 = \bar{r}^2 + \bar{z}^2; \quad c = [4\pi\mu_\alpha(1-\nu_\alpha)]^{-1} \\ &\bar{m} = \frac{2rr_i}{\bar{R}^2}; \quad m_1 = 1 - \bar{m} \end{aligned} \tag{55}$$

and $K(\bar{m})$ and $E(\bar{m})$ are, respectively, the complete elliptic integrals of the first and second-kinds and r_i and z_i refer to the coordinates of a field point. The corresponding terms for $P_{lk}^{*(\alpha)}$ can be obtained by the substitution of (51)–(54) in (47).

Upon discretization of the boundaries Γ_α into boundary elements (Fig. 10), the integral equation (49) can be represented in the form:

$$\begin{pmatrix} \mathbf{H}^{(\alpha)} & \mathbf{H}_I^{(\alpha)} \end{pmatrix} \begin{pmatrix} \mathbf{u}^{(\alpha)} \\ \mathbf{u}_I^{(\alpha)} \end{pmatrix} = \begin{pmatrix} \mathbf{M}^{(\alpha)} & \mathbf{M}_I^{(\alpha)} \end{pmatrix} \begin{pmatrix} \mathbf{P}^{(\alpha)} \\ \mathbf{P}_I^{(\alpha)} \end{pmatrix}, \tag{56}$$

where $\mathbf{H}$s and $\mathbf{M}$s are the influence coefficient matrices derived from the integration of the fundamental solutions $P_{lk}^{*(\alpha)}$ and $u_{lk}^{*(\alpha)}$, respectively. In the instance where there is complete bonding at the fibre–matrix interface, we have

$$\mathbf{u}_I^{(f)} = \mathbf{u}_I^{(m)} = \mathbf{u}_I; \quad \mathbf{P}_I^{(f)} = -\mathbf{P}_I^{(m)} = \mathbf{P}_I. \tag{57}$$

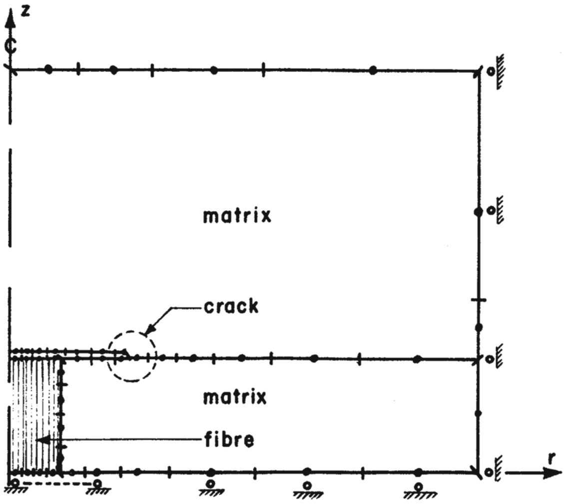

Fig. 10 Boundary element discretization of the fibre and penny-shaped crack region

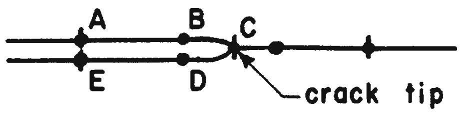

Fig. 11 Boundary element modelling of the crack tip

Using the above result, the complete matrix equation governing the fibre composite–crack interaction problem can be expressed in the form

$$\begin{pmatrix} \mathbf{H}^{(f)} & \mathbf{H}_I^{(f)} & \mathbf{0} \\ \mathbf{0} & \mathbf{H}_I^{(m)} & \mathbf{H}^{(m)} \end{pmatrix} \begin{pmatrix} \mathbf{u}^{(f)} \\ \mathbf{u}_I \\ \mathbf{u}^{(m)} \end{pmatrix} = \begin{pmatrix} \mathbf{M}^{(f)} & \mathbf{M}_I^{(f)} & \mathbf{0} \\ \mathbf{0} & \mathbf{M}_I^{(m)} & \mathbf{M}^{(m)} \end{pmatrix} \begin{pmatrix} \mathbf{P}^{(f)} \\ \mathbf{P}_I \\ \mathbf{P}^{(m)} \end{pmatrix}. \tag{58}$$

5.2 The modelling of crack tip behaviour

In the boundary element discretizations discussed in the preceding section, quadratic elements are used to model the boundaries of the matrix and fibre regions. This allows the variation of displacements and tractions within the element to be described by

$$\left\{ \begin{matrix} u_i^{(\alpha)} \\ P_i^{(\alpha)} \end{matrix} \right\} = a_0 + a_1\zeta + a_2\zeta^2, \tag{59}$$

where ζ is the local coordinate of the element and a_r $(r = 0, 1, 2)$ are constants of interpolation. In the context of linear elastic fracture mechanics, however, the stress field at the crack tip should contribute to a $1/\sqrt{r}$-type stress singularity. In the application of the conventional finite element technique to the study of crack problems, the quarter point of the type proposed in [99] can be used to incorporate the required $\sqrt{r}$-type variations in the displacements:

$$\left\{ \begin{matrix} u_i^{(\alpha)} \\ P_i^{(\alpha)} \end{matrix} \right\} = b_0 + b_1\sqrt{r} + b_2 r. \tag{60}$$

If elements with variations of the type (60) are incorporated in the boundary element scheme, the $P_i^{(\alpha)}$ in (60) does not produce a $1/\sqrt{r}$-type stress singularity at the crack tip. The approach adopted in [93,94] is to incorporate

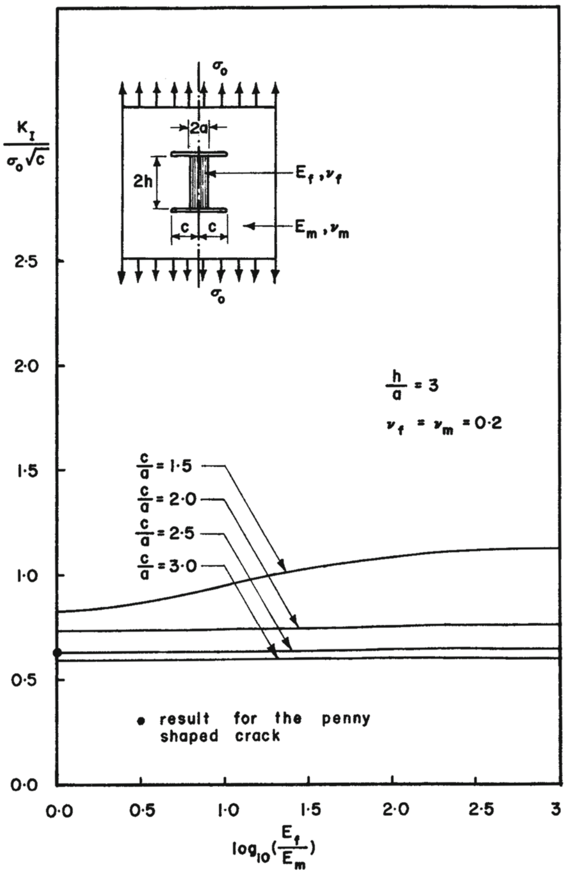

Fig. 12 Mode I stress intensity factor at the *tip* of the cracks at the extremities of the finite fibre

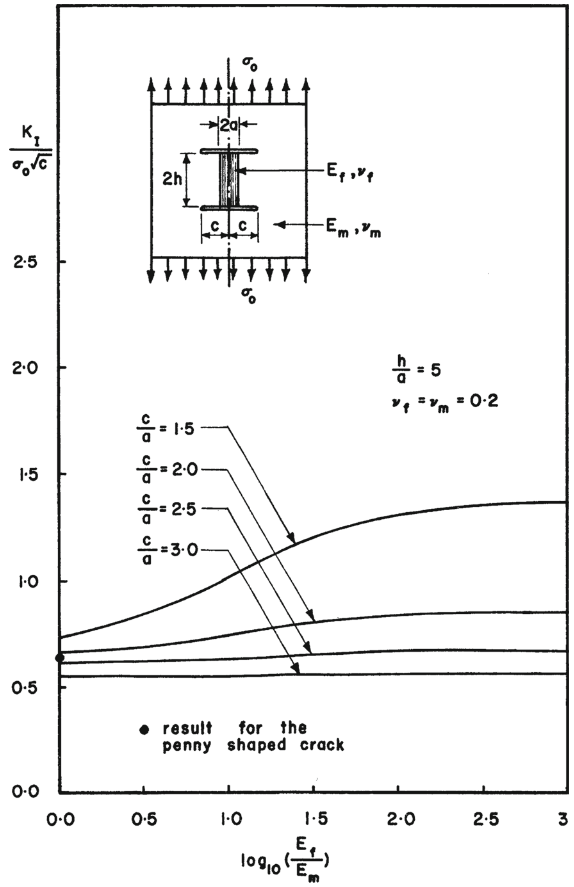

Fig. 13 Mode I stress intensity factor at the *tip* of the cracks at the extremities of the finite fibre

a singular traction quarter point boundary element, where the traction variations in (60) are multiplied by a non-dimensional $\sqrt{l/r}$, where l is the length of the crack tip element. The variations of tractions can be expressed in the form:

$$P_i = \frac{c_0}{\sqrt{r}} + c_1 + c_2\sqrt{r}, \tag{61}$$

where b_i and c_i $(i = 0, 1, 2)$ are constants. The performance of both types of quarter-point elements has been studied extensively in the literature on boundary element treatment of crack problems [41,93,96,100–103]. The boundary element technique was also used recently by Perelmuter [104] to examine the problem of a bridged plane crack located at a bi-material region.

In the crack–fibre interaction problems examined in this paper, the axial straining induces a state of axial symmetry in the fibre–matrix composite region. Consequently, only the Mode I and Mode II stress intensity factors are present at the tips of the penny-shaped crack region (Fig. 9). The crack-opening mode stress intensity factor can be evaluated by applying the displacement correlation method, which utilizes the nodal displacements at four locations A, B, E, and D and the crack tip (Fig. 11). The Mode I stress intensity factor can be obtained from the result:

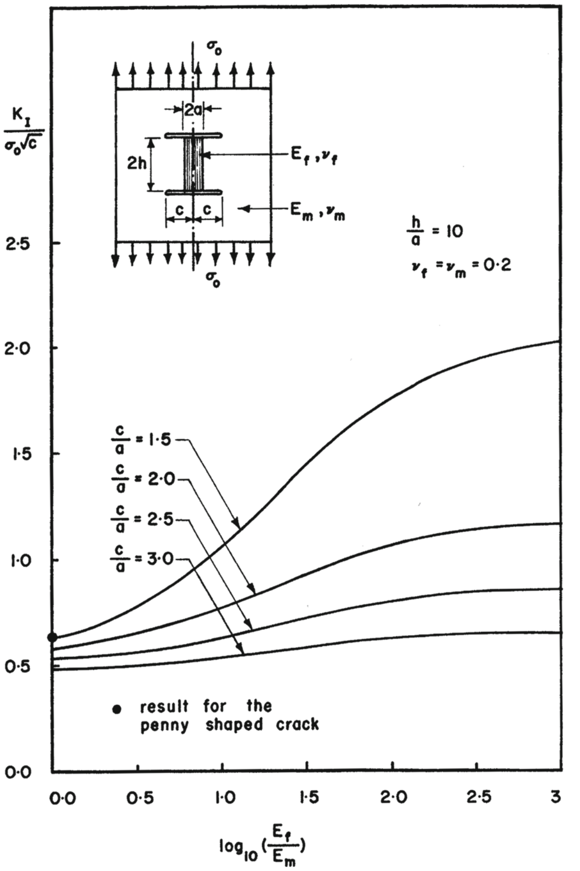

Fig. 14 Mode I stress intensity factor at the *tip* of the cracks at the extremities of the finite fibre

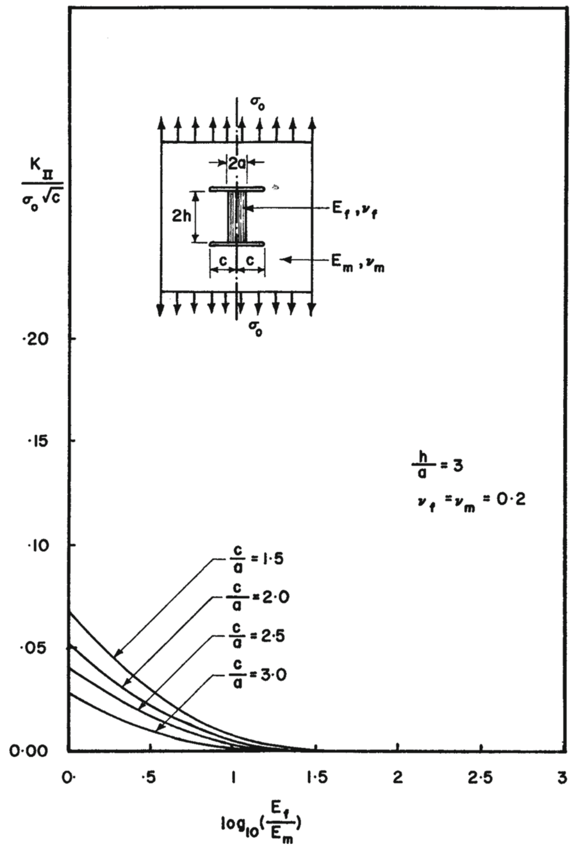

Fig. 15 Mode II stress intensity factor at the *tip* of the cracks at the extremities of the finite fibre

$$K_{\mathrm{I}}^{(\alpha)} = \frac{\mu_\alpha}{(k_\alpha + 1)}\sqrt{\frac{2\pi}{l_0}}\Big\{4[u_z(B) - u_z(D)] + [u_z(E) - u_z(A)]\Big\}, \tag{62}$$

where $k_\alpha = (3 - 4\nu_\alpha)$ and l_0 is the length of the crack tip element. Similarly, the crack-shearing mode stress intensity factor can be obtained from the result:

$$K_{\mathrm{II}}^{(\alpha)} = \frac{\mu_\alpha}{(k_\alpha + 1)}\sqrt{\frac{2\pi}{l_0}}\Big\{4[u_r(B) - u_r(D)] + u_r(E) - u_r(A)\Big\}. \tag{63}$$

5.3 Numerical results

Considering the symmetry of the fibre–crack interaction problem about the plane $z = 0$, it is sufficient to consider a boundary element discretization, which is restricted to the region $z \geq 0$. Figure 10 shows the boundary element discretization, and the accuracy of the boundary element modelling has been verified through comparisons with the exact analytical solution for the Mode I stress intensity factor for a penny-shaped crack located in an elastic solid of infinite extent and subjected to a uniform axial stress and given by the result (43). The boundary element scheme

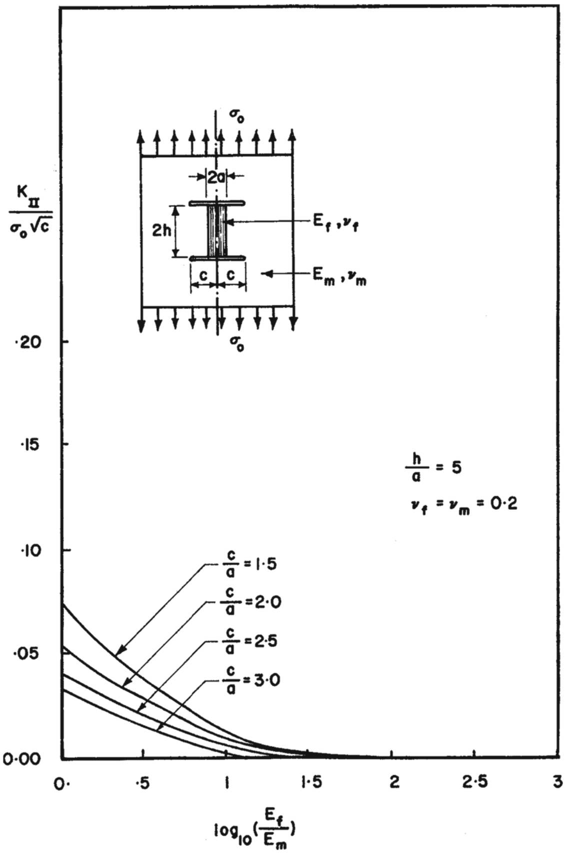

Fig. 16 Mode II stress intensity factor at the *tip* of the cracks at the extremities of the finite fibre

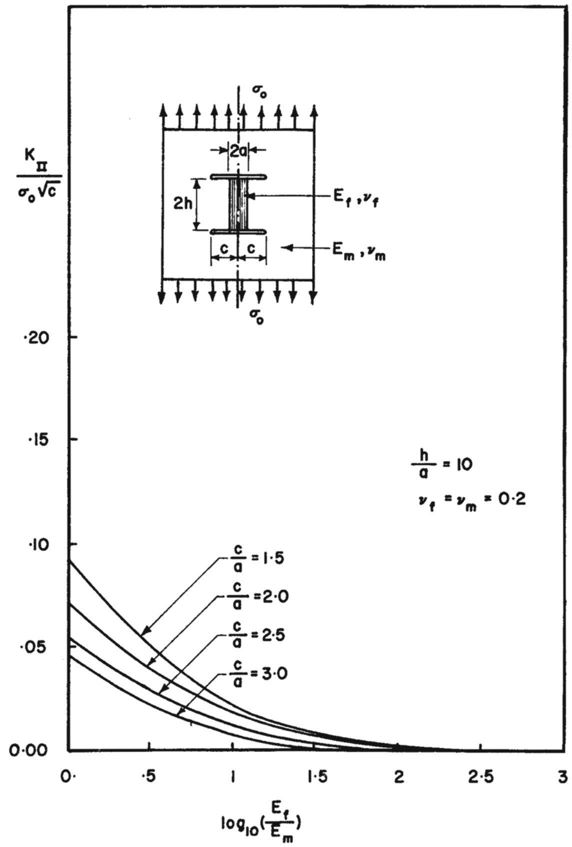

Fig. 17 Mode II stress intensity factor at the *tip* of the cracks at the extremities of the finite fibre

provides numerical estimates for the stress intensity factor to an accuracy of less than 5 %, and the accuracy can be improved by increasing the element numbers used in the boundary element discretization.

In the numerical evaluation of the stress intensity factors at the penny-shaped cracks located at the extremities of the fibre, several factors need to be taken into consideration; these include (i) the aspect ratio of the fibre h/a, (ii) the radius of the crack in relation to the radius of the fibre c/a, (iii) Poisson's ratios of the matrix and fibre materials ν_m, ν_f and (iv) the fibre/matrix modular ratio E_f/E_m. In the presentation of numerical results, the above parameters are restricted to the following ranges: $h/a \in (3,\ 10)$; $c/a \in (1.5,\ 3.0)$; $\nu_m = \nu_f = 0.2$; and $E_f/E_m \in (1,\ 10^3)$.

Figures 12, 13 and 14 illustrate the variations in the Mode I stress intensity factor at the crack tip. From the results shown in Fig. 14, it is evident that as the modular ratio $E_f/E_m \to 1$, $c/a > 1$ and when $h/a > 10$, the interaction between the cracks at the extremities of the fibre inclusion is less significant and we obtain from the numerical results, the relevant stress intensity factor for the classical penny-shaped crack in an elastic solid of infinite extent. As h/a becomes small (in the range of 3–5), the interaction between the cracks influences the result for $K_{\rm I}$ even for the case when $E_f/E_m \to 1$ and $c/a > 1$. The results of the numerical investigations also indicate that an increase in the modular ratio E_f/E_m has the effect of amplifying the Mode I stress intensity factor at the crack tip. This amplification effect becomes particularly significant as h/a increases and as $c/a \to 1$. It should, however, be noted that as $c/a \to 1$, the crack tip is located at a bi-material interface and the conventional boundary element modelling of the crack tip that incorporates a $1/\sqrt{r}$-type stress singularity cannot accommodate the oscillatory form of the stress singularity that will be present at a bi-material point [105–107]. In such cases, the boundary element technique should be modified to accommodate the oscillatory form of the stress singularity, and approaches for such modelling are given in [108–112]. Figures 15, 16 and 17 illustrate the influence of the geometric and material parameters on the Mode II stress intensity factor at the crack tip. It is evident that the Mode II stress intensity factor at the crack tip is considerably smaller than the corresponding Mode I stress intensity factor, which suggests that the penny-shaped crack is most likely to extend in a self-similar fashion when the crack tip attains K_{IC}, the critical stress intensity factor. The effects of the Mode II stress intensity factor become appreciable only as $E_f/E_m \to 1$. For values of $E_f/E_m > 10^2$, the stiffness of the cylindrical inclusion is sufficient to suppress the Mode II stress intensity factor for all choices of h/a and c/a. These conclusions should take into consideration the specific values of Poisson's ratios assigned to the fibre and matrix materials in developing the computational results.

6 Concluding remarks

Ideally, fibre-reinforced materials are assumed to be defect free. Defects can, however, be introduced either during the manufacture of the composite or during its use, due to impact and thermal loadings, loss of bonding between the reinforcing fibres and the matrix, and as a result of chemical action and moisture migration. In these situations, the fibres can remain intact with delamination at the fibre–matrix interface, and this leads to the process of flaw bridging. The influence of flaw bridging can be important since the load carrying capacity and stress state at the fibre–matrix delaminated region can be moderated by the presence of fibre continuity. The paper reviews the topic of flaw bridging and presents examples of idealized three-dimensional bridged defects in unidirectionally fibre-reinforced materials, and either the stress amplification at the boundary of the delaminated region or the stress intensity factor at the boundary of a penny-shaped defect can be suppressed by the bridging action of the fibres. These observations are applicable to situations where loadings are applied in the direction of the bridging fibres and, due to the flexible nature of the bridging fibres, the suppression of stress amplification or stress intensity factors will not occur for the other forms of external loadings of the defect. The computational analysis of the isolated fibre problem containing penny-shaped cracks at the ends of the finite fibres indicates that reinforcing action can lead to amplification of the Mode I stress intensity factor at the end cracks, particularly as the crack diameter approaches that of the fibre diameter. It could be concluded that, while fibre continuity can lead to the suppression of stress amplification at defects in continuously reinforced composites, the converse can occur at cracks located at the ends of isolated fibres.

Acknowledgments The work described in this paper was supported by a Discovery Research Grant awarded by the Natural Sciences and Engineering Research Council of Canada. The author is indebted to the reviewers for their substantial constructive comments.

Appendix

The expressions for the constants $\bar{K}$, $\bar{G}$, $\bar{E}$, $\bar{\nu}$ and $\bar{G}^*$ are given by Hashin and Rosen [48] as follows:

$$\overline{K} = \left\{ \frac{\xi_0(1 + 2\nu_m V_f) + 2\nu_m V_m}{\xi_0 V_m + V_f + 2\nu_m} \right\}(\lambda_m + G_m), \quad \overline{G} = \left\{ \frac{(\alpha + \beta_m V_f)(1 + \rho V_f^3) - 3V_f V_m^2 \beta_m^2}{(\alpha - V_f)(1 + \rho V_f^3) - 3V_f V_m^2 \beta_m^2} \right\} G_m,$$

$$\overline{\nu} = \left\{ \frac{V_f E_f L_1 + V_m E_m L_2 \nu_m}{V_f E_f L_3 + V_m E_m L_2} \right\}, \quad \overline{G}^* = \left\{ \frac{\eta(1 + V_f) + V_m}{\eta V_m + V_f + 1} \right\} G_m$$

and

$$\bar{E} = V_f E_f + V_m E_m,$$

where

$$L_1 = 2\nu_f(1 - \nu_m^2)V_f + \nu_m(1 + \nu_m)V_m; \quad L_2 = 2(1 - \nu_f^2)V_f,$$

$$L_3 = 2(1 - \nu_m^2)V_f + (1 + \nu_m)V_m,$$

$$\xi_0 = \frac{\lambda_f + G_f}{\lambda_m + G_m}; \quad \alpha = \frac{\eta + \beta_m}{\eta - 1}; \quad \rho = \frac{\beta_m - \eta\beta_f}{1 + \eta\beta_f},$$

$$\eta = \frac{G_f}{G_m}; \quad V_m + V_f = 1,$$

$$G_i = \frac{E_i}{2(1+\nu_i)}; \quad \lambda_i = \frac{\nu_i E_i}{(1+\nu_i)(1-2\nu_i)}; \quad \beta_i = \frac{1}{3-4\nu_i}; \quad (i = m, f).$$

References

1. Backlund J (1981) Fracture analysis of notched composites. Comput Struct 13:145–154
2. Kelly A (1970) Interface work and the work of fracture of a fibrous composite. Proc R Soc A 319:95–116
3. Aveston J, Kelly A (1980) Tensile first cracking strain and strength of hybrid composites and laminates. Philos Trans R Soc A 294:519–534
4. Bowling J, Groves GW (1979) The propagation of cracks in composites consisting of ductile wires in a brittle matrix. J Mater Sci 14:443–449
5. Sih GC (1979) Fracture mechanics of composite materials. In: Sih GC, Tamusz VP (eds) Fracture mechanics of composite materials, Proc 1st USA-USSR Symp. Sijthoff and Noordhoff, Alphen aan den Rijn, The Netherlands, pp 111–130
6. Beaumont PWR, Harris B (1972) The energy of crack propagation in carbon fibre-reinforced resin systems. J Mater Sci 7:1265–1279
7. Beaumont PWR (1979) Fracture mechanisms in fibrous composite. In: Smith RA (ed) Fracture mechanics: current status and future prospects. Pergamon Press, New York, pp 211–233
8. Selvadurai APS (1981) A theoretical model for elastic flaw bridging in unidirectional fibre-reinforced composites. In: Selvadurai APS (eds) Mechanics of structured media. Proceedings of the international symposium on mechanics of structured media. Developments in Mechanics, vol 5A. Elsevier Scientific Publishers, Amsterdam, pp 59–72
9. Selvadurai APS (1983) Concentrated body force loading of an elastically bridged penny-shaped flaw in a unidirectional fibre-reinforced composite. Int J Fract 21:149–159
10. Stang H (1987) A double inclusion model for microcrack arrest in fibre-reinforced brittle materials. J Mech Phys Solids 35:325–342
11. Rose LRF (1987) Crack reinforcement by distributed springs. J Mech Phys Solids 35:383–405
12. McCartney LN (1987) Mechanics of matrix cracking in brittle-matrix fibre-reinforced composites. Proc R Soc A Math Phys 409:329–350
13. Budiansky B, Hutchinson JW, Evans AG (1986) Matrix fracture in fibre-reinforced ceramics. J Mech Phys Solids 34:167–189
14. Budiansky B, Amazigo JC (1989) Toughening by aligned, frictionally constrained fibers. J Mech Phys Solids 37:93–109
15. Movchan NV, Willis JR (1996) Critical load for a mode-1 crack reinforced by bridging. Q J Mech Appl Math 49:545–564
16. Movchan NV, Willis JR (1998) Penny-shaped crack bridged by fibres. Q Appl Math 56:327–340
17. Ballarini R, Muju S (1991) Stability analysis of bridged cracks in brittle matrix composites. ASME Paper No 91-GI-094
18. Bažant ZP, Bittnar Z, Jirasek M, Mazars J (eds) (1994) Fracture and damage in quasi-brittle structures. E & FN Spon, London
19. Zhang J, Stang H, Li VC (2001) Crack bridging model for fibre reinforced concrete under fatigue cycling. Int J Fatigue 23:655–670
20. Bažant ZP (2005) Scaling of structural strength, 2nd edn. Elsevier-Butterworth, London
21. Maso JC (ed) (2005) Interfacial transition zone in concrete. E & FN Spon, London
22. Bentur A, Mindess S (2007) Fibre reinforces cementitious composites. E & FN Spon, London
23. Carpinteri A, Puzzi S (2007) The bridged crack model for the analysis of brittle matrix fibrous composites under repeated bending loading. J Appl Mech 74:1239–1246
24. de Silva FA, Mobasher B, Soranakon C (2011) Effect of fiber shape and morphology on interfacial bond and cracking behaviours of sisal fiber cement based composites. Cem Concr Compos 33:814–823
25. Selvadurai APS (1983) On three-dimensional fibrous flaws in unidirectional fibre-reinforced elastic composites. J Appl Math Phys (ZAMP) 34:51–64
26. Chen WT (1968) Axisymmetric stress field around spheroidal inclusions and cavities in a transversely isotropic material. J Appl Mech Trans ASME 35:770–773
27. Atkinson C (1970) An iterative scheme for solving problems relating to cracks opening under displacement dependent internal stress. Int J Fract 6:193–198
28. Selvadurai APS (2010) Crack-bridging in a unidirectionally fibre-reinforced plate. J Eng Math 68:5–14
29. Selvadurai APS (2010) On the mode I stress intensity factor for an external circular crack with fibre-bridging. Compos Struct 92:1512–1516
30. Selvadurai APS, Rajapakse RKND (1990) Axial stiffness of anchoring rods embedded in elastic media. Can J Civ Eng 17:321–328
31. Clyne TW, Withers PJ (1995) An introduction to metal matrix composites. Cambridge University Press, Cambridge
32. Selvadurai APS (1994) Matrix crack extension at a frictionally constrained fibre. J Eng Mater Tech ASME 119:398–402

33. Pacella AH, Erdogan F (1974) A penny-shaped crack in a filament reinforced matrix II. The crack problem. Int J Solids Struct 10:807–819
34. Wijeywickrema AC, Keer LM, Hirashima K, Mura T (1991) The annular crack surrounding an elastic fiber in a tension field. Int J Solids Struct 27:315–328
35. Wijeywickrema AC, Keer LM (1992) Matrix crack interaction in a fiber-reinforced brittle matrix composite. Int J Solids Struct 29:559–570
36. Wijeywickrema AC, Keer LM (1993) Matrix cracking in a fiber-reinforced composite with slip at the fiber-matrix interface. Int J Solids Struct 30:91–113
37. Taya M, Mura T (1981) On the stiffness and strength of an aligned short-fibre reinforced composite containing fiber-end cracks under uniaxial applied stress. J Appl Mech ASME 48:361–367
38. Selvadurai APS, Au MC, Singh BM (1996) The matrix-fibre crack in an elastic solid. J Appl Mech 118:639–649
39. ten Busschen A, Selvadurai APS (1995) Mechanics of the segmentation of an embedded fibre, part I: experimental investigations. J Appl Mech ASME 62:87–97
40. Selvadurai APS, ten Busschen A (1995) Mechanics of the segmentation of an embedded fibre, part II: computational modelling and comparisons. J Appl Mech ASME 62:98–107
41. Selvadurai APS (2000) Fracture evolution during indentation of a brittle elastic solid. Mech Cohesive-Frict Mat 5:325–339
42. Selvadurai APS, Nikopour H (2012) Transverse elasticity of a unidirectionally reinforced composite with an irregular fibre arrangement: Experiments, theory and computations. Compos Struct 94:1973–1981
43. Spencer AJM (1972) Deformations of fibre-reinforced materials. Clarendon Press, Oxford
44. Spencer AJM (1979) On the stress intensity factor for a crack in a highly anisotropic plate. Q J Mech Appl Math 32:437–444
45. Spencer AJM (1981) Continuum models of fibre-reinforced materials. In: Selvadurai APS (ed) Mechanics of Structured Media. Proceedings of the international symposium on mechanics of structured media. Developments in Mechanics, vol 5A. Elsevier Scientific Publ, Amsterdam, pp 3–26
46. Spencer AJM (ed) (1984) Continuum theory of the mechanics of fibre-reinforced composites. CISM courses and lectures no. 282. Springer, Wien
47. Hill R (1964) Theory of mechanical properties of fibre-strengthened materials: I. Elastic behaviour. J Mech Phys Solids 12:199–212
48. Hashin Z, Rosen BW (1964) The elastic moduli of fibre-reinforced materials. J Appl Mech 31:223–232
49. Hale DK (1976) The physical properties of composite materials. J Mater Sci 11:2105–2141
50. Christensen RM (1979) Mechanics of composite materials. Wiley, New York
51. Elliott HA (1949) Three-dimensional stress distributions in hexagonal aeolotropic crystals. Proc Camb Philos Soc 45:621–630
52. Shield RT (1951) Note on problems in hexagonal aeolotropic materials. Proc Camb Philos Soc 47:401–409
53. Lekhnitskii SG (1963) Theory of elasticity of an anisotropic elastic body. Holden-Day Inc, San Francisco
54. Green AE, Zerna W (1968) Theoretical elasticity. Clarendon Press, Oxford
55. Sack RA (1946) Extension of Griffith's theory of rupture to three dimensions. Proc Phys Soc 58:729–736
56. Sneddon IN (1945) The distribution of stress in the neighbourhood of a crack in an elastic solid. Proc R Soc A Math Phys 187:229–260
57. Liebowitz H (1968) Fracture I–IV. Academic Press, New York
58. Sih GC (1974) Mechanics of fracture, I–V. Noordhoff International, Leyden
59. Cherepanov GP (1979) Mechanics of brittle fracture. McGraw-Hill, New York
60. Sneddon IN (1951) Fourier transforms. McGraw-Hill, New York
61. Selvadurai APS (2000) Partial differential equations in mechanics, vol. 2: the biharmonic equation, Poisson's equation. Springer, Berlin
62. Mikhlin SG (1957) Singular integral equations. Pergamon Press, Oxford (Engl. Transl. Ed. Armstrong AH)
63. Adkins JE, Rivlin RS (1955) Large elastic deformations of isotropic materials X. Reinforcement by inextensible cords. Philos Trans R Soc A 248:201–223
64. Everstine GC, Pipkin AC (1971) Stress channelling in transversely isotropic elastic composites. J Appl Math Phys (ZAMP) 22:825–834
65. England AH, Rogers TG (1973) Plane crack problems for ideal fibre-reinforced materials. Q J Mech Appl Math 26:303–320
66. Pipkin AC, Rogers TG (1971) Plane deformations of incompressible fibre-reinforced materials. J Appl Mech ASME 38:634–640
67. Spencer AJM (1974) Boundary layers in highly anisotropic plane elasticity. Int J Solids Struct 10:1103–1123
68. Sanchez V, Pipkin AC (1978) Crack tip analysis for elastic materials reinforced with strong fibres. Q J Mech Appl Math 31:349–362
69. Morland LW (1973) A plane theory of inextensible transversely isotropic elastic composites. Int J Solids Struct 9:1501–1518
70. Pipkin AC (1982) Cracks in inextensible materials. Proceedings of the 9th US national congress applied mechanics. Cornell University, Ithaca, ASME 231–235
71. Spencer AJM, Soldatos KP (2007) Finite deformations of fibre-reinforced elastic solid with fibre bending stiffness. Int J Nonlinear Mech 42:355–368
72. Soldatos KP (2010) Second-gradient plane deformations of ideal fibre-reinforced materials: implications of hyper-elasticity theory. J Eng Math 68(1):99–127
73. Soldatos KP (2013) Foundation of polar linear elasticity for fibre-reinforced materials. J Elast 114(2):155–178
74. Baker CTH (1977) The numerical treatment of integral equations. Clarendon Press, Oxford
75. Delves LM, Mohamed JL (1985) Computational methods for integral equations. Cambridge University Press, Cambridge

76. Atkinson KE (1997) The numerical solution of integral equations of the second kind. Cambridge University Press, Cambridge
77. Selvadurai APS (1993) The axial loading of a rigid circular anchor plate embedded in an elastic halfspace. Int J Numer Anal Methods Geomech 17:343–353
78. Selvadurai APS (2000) An inclusion at a bi-material elastic interface. J Eng Math 37:155–170
79. Selvadurai APS (2001) On the displacements of an elastic halfspace containing a rigid inhomogeneity. Int J Geomech 1:149–174
80. Selvadurai APS (2002) Mechanics of a rigid circular disc bonded to a cracked elastic halfspace. Int J Solids Struct 39:6035–6053
81. Selvadurai APS (1979) The interaction between a uniformly loaded circular plate and an isotropic elastic halfspace. J Struct Mech 7:231–246
82. Selvadurai APS (1979) An energy estimate of the flexural deflections of a circular foundation embedded in an elastic medium. Int J Numer Anal Methods Geomech 3:285–292
83. Selvadurai APS (2007) On adhesion energy estimates derived from the pressurized brittle delamination of a flexible thin film. Acta Materialia 55:4679–4687
84. Selvadurai APS, Labanieh S, Boulon MJ (2007) Mechanics of contact between a flexible transducer diaphragm located at a rigid boundary and an elastic material. Int J Num Anal Methods Geomech 31:933–952
85. Selvadurai APS, Dumont NA (2011) Mindlin's problem for a halfspace indented by a flexible plate. J Elast 105:253–269
86. Spencer AJM (1965) A theory of failure of ductile materials reinforced by elastic fibres. Int J Mech Sci 7:197–209
87. Sih GC, Tamusz VP (Eds) (1979) Fracture of composite materials. Proceedings of the1st USA-USSR Symposium, Sijthoff and Noordhoff, Alphen aan den Rijn
88. Hashin Z, Herakovich CT (eds) (1983) Mechanics of composite materials: recent advances. Proceedings of the IUTAM symposium on mechanics of composite materials, Blacksburg. Pergamon Press, Oxford
89. Kelly A, Rabotnov YuN (eds) (1983) Handbook of composites, vol 1–4. North-Holland, Amsterdam
90. Mura T (1982) Micromechanics of defects in solids. Martinus Nijhoff Publ, The Hague
91. Nemat-Nasser S, Hori M (1993) Micromechanics: overall properties of heterogeneous materials. Martinus Nijhoff, New York
92. Brebbia CA, Telles JCF, Wrobel LC (1984) Boundary element techniques. Springer, Berlin
93. Cruse TA, Wilson RB (1977) Boundary integral equation method for elastic fracture mechanics AFSOR-TR-78-0355, 10–11
94. Blandford GE, Ingraffea AR, Liggett JA (1981) Two-dimensional stress intensity factor computations using the boundary element method. Int J Numer Methods Eng 17:387–404
95. Kermanidis Th (1975) Numerical solution of axially symmetric elasticity problems. Int J Solids Struct 1:495–500
96. Aliabadi MH (1997) Boundary element formulations in fracture mechanics. Appl Mech Rev 50:83–96
97. Katsikadelis JT (2002) Boundary elements: theory and applications. Elsevier Sci. Publ, Amsterdam
98. Hartmann F (1980) Computing the C-matrix in non-smooth boundary points. In: Brebbia CA (ed) New developments in BEM. CML Southampton, Butterworth, London, pp 367–379
99. Barsoum RS (1976) On the use of isoparametric finite elements in linear fracture mechanics. Int J Numer Methods Eng 10:25–37
100. Tan CL, Selvadurai APS (1986) Internally indented penny-shaped cracks: a comparison of analytical and boundary integral equation estimates. Theor Appl Fract Mech 5:181–188
101. Selvadurai APS, Au MC (1988) Cracks with frictional surfaces: a boundary element approach. In: Brebbia CA (ed) Proceedings of the 9th boundary element conference, Southampton. Springer, Berlin, pp 211–230
102. Selvadurai APS, Au MC (1989) Crack behaviour associated with contact problems with non-linear interface constraints. In: Brebbia CA, Zamani N (eds) Boundary element techniques: applications in engineering. Computational Mechanics Publications, Southampton
103. Selvadurai APS (1996) On integral equation approaches to the mechanics of fibre–crack interaction. Eng Anal Bound Elem 17:287–294
104. Perelmuter MN (2012) Boundary element analysis of stress state at the bridged zone of an interface crack. Comput Cont Mech 5:415–426
105. Rice JR, Sih GC (1965) Plane problems of cracks in dissimilar media. J Appl Mech 32:418–423
106. England AH (1971) On stress singularities in linear elasticity. Int J Eng Sci 9:571–585
107. Atkinson C (1979) Stress singularities and fracture mechanics. Appl Mech Rev 32:123–135
108. Lee KY, Choi HJ (1988) Boundary element analysis of stress intensity factors for bi-material interface cracks. Eng Fract Mech 29:461–472
109. Yuuki R, Cho SB (1988) Boundary element analysis of stress intensity factors for an interface crack in dissimilar materials. In: Cruse TA, Tanaka M (eds) Boundary element methods in applied mechanics. Pergamon Press, New York, pp 179–190
110. Tan CL, Gao YL (1991) Determination of characterizing parameters of bi-material interface cracks using the boundary element method. Eng Fract Mech 36:919–932
111. Tan CL, Gao YL (1991) Axisymmetric boundary integral equation analysis of interface cracks between dissimilar materials. Comput Mech 7:387–396
112. Gao YL, Tan CL, Selvadurai APS (1992) Stress intensity factors for cracks around or penetrating an elliptical inclusion using the boundary element method. Eng Anal Bound Elem 10:59–68